

Submitted to ApJ

The Unusual Tidal Dwarf Candidate in the Merger System NGC 3227/6: Star Formation in a Tidal Shock?

Carole G. Mundell¹

*Astrophysics Research Institute, Liverpool John Moores University, Twelve Quays House,
Egerton Wharf, Birkenhead, CH41 1LD, U.K.*

cgm@astro.livjm.ac.uk

Phil A. James

*Astrophysics Research Institute, Liverpool John Moores University, Twelve Quays House,
Egerton Wharf, Birkenhead, CH41 1LD, U.K.*

paj@astro.livjm.ac.uk

Nora Loiseau

XMM-Newton Science Operations Center, VILSPA, Apartado 50727, 28080 Madrid, Spain

nloiseau@xmm.vilspa.esa.es

Eva Schinnerer²

National Radio Astronomy Observatory, P.O. Box 0, Socorro, NM 87801-0387

eschinnerer@nrao.edu

and

Duncan A. Forbes

*Centre for Astrophysics and Supercomputing, Swinburne University of Technology, Mail
Number 31, P.O. Box 218, Hawthorn, VIC 3122, Australia*

dforbes@astro.swin.edu.au

¹Royal Society University Research Fellow

²Jansky Postdoctoral Fellow at the National Radio Astronomy Observatory

ABSTRACT

We report the discovery of active star formation in the H I cloud associated with the interacting Seyfert system NGC 3227/NGC 3226 that was originally identified as a candidate tidal dwarf galaxy (TDG) by Mundell et al. and that we name J1023+1952. We present broad-band optical B, R, I (from the INT) and ultraviolet images (from XMM-Newton) that show the H I cloud is associated with massive on-going star formation seen as a cluster of blue knots ($M_B \lesssim -15.5$ mag) surrounded by a diffuse ultraviolet halo and co-spatial with a ridge of high neutral hydrogen column density ($N_H \sim 3.7 \times 10^{21} \text{ cm}^{-2}$) in the southern half of the cloud. We also detect H α emission from the knots with a flux density of $F_{H\alpha} \sim 2.55 \times 10^{-14} \text{ erg s}^{-1} \text{ cm}^{-2}$ corresponding to a star-formation rate of $\text{SFR}(H_{H\alpha}) \sim 10.6 \times 10^{-3} M_\odot \text{ yr}^{-1}$. J1023+1952 lies at the base of the northern tidal tail, and, although it spatially overlaps the edge of the disk of NGC 3227, Mundell et al. showed that the H I cloud is kinematically distinct with an H I mean velocity 150 km s^{-1} higher than that of NGC 3227. Comparison of ionized (H α) and neutral (H I) gas kinematics of the cloud show closely matched recessional velocities, providing strong evidence that the star-forming knots are embedded in J1023+1952 and are not merely optical knots in the background disk of NGC 3227, thus confirming J1023+1952 as a gas-rich ($M_H/L_B > 1.5$) dwarf galaxy. No star formation is detected in the northern half of the cloud, despite similar H I column densities; instead, our new high resolution H I image shows a ridge of high column density coincident with the reddest structures evident in our B–I image. We suggest these structures are caused by the background stellar continuum from the disk of NGC 3227 being absorbed by dust intrinsic to J1023+1952, thus placing J1023+1952 in front of NGC 3227 along the line of sight. We discuss two scenarios for the origin of J1023+1952; as a third, pre-existing dwarf galaxy involved in the interaction with NGC 3227 and NGC 3226, or a newly-forming dwarf galaxy condensing out of the tidal debris removed from the gaseous disk of NGC 3227. The first scenario is feasible given that NGC 3227 is the brightest member of a galaxy group, an environment in which pre-existing dwarf galaxies are expected to be common. However, the lack of a detectable old stellar population in J1023+1952 makes a tidal origin more likely. If J1023+1952 is a bound object forming from returning gaseous tidal tail material, its unusual location at the base of the northern tail implies a dynamically young age similar to its star-formation age, and suggests it is in the earliest stages of TDG evolution. Whatever the origin of J1023+1952 we suggest that its star formation is shock-triggered by collapsing tidal debris.

Subject headings: galaxies: individual (NGC 3227) — galaxies: Seyfert — galaxies: interactions — galaxies: dwarf

1. INTRODUCTION

The importance of collisions between galaxies as a key driver of galaxy formation and evolution is well recognized, with the galaxy merger rate being higher in the early Universe (Burkey et al. 1994; Struck 1999) and galaxies undergoing several interactions, of varying strengths, in their lifetime. Dwarf galaxies in particular are thought to play an important role in galactic formation and evolution but the origin of today’s dwarf galaxies is still debated; cold dark matter hierarchical models invoke the merger of small dark matter halos formed in the early Universe to produce larger galaxies while alternative ‘down-sizing’ models suggest large galaxies formed first via collapse of primordial gas clouds and smaller galaxies were created later, perhaps through tidal interaction (Cowie et al. 1996; Hunter, Hunsberger & Roye 2000). Indeed, as many as one-half of the current dwarf galaxy population of compact groups could have formed from the interaction of giant spiral galaxies (Hunsberger, Charlton & Zaritsky 1996).

Tidal forces between interacting galaxies redistribute galactic material, producing extensive stellar and gaseous tidal tails (e.g. Toomre & Toomre 1972; Barnes & Hernquist 1992; Mihos 2001); tidal dwarf galaxies (TDG) are small, gas-rich galaxies formed from gas removed from the progenitor galaxy disks either as coherent gas clouds ejected during the encounter (Elmegreen, Kaufman & Thomasson 1993) or via the gravitational collapse of tidal debris (Zwicky 1956; Duc et al. 2000). As nearby galaxies in the process of formation, TDGs offer an important laboratory to study the ongoing processes of galaxy evolution and the link with tidal interaction, but to date only a small number have been confirmed and studied in detail (e.g. Braine et al. 2001).

NGC 3227 is a nearby Seyfert galaxy that is interacting with a gas-poor dwarf elliptical companion NGC 3226. Neutral hydrogen (HI) imaging of the system (Mundell et al. 1995) revealed tidal tails extending $\gtrsim 100$ kpc north and south of the disk of NGC 3227 and well-ordered gas in the disk of NGC 3227; no HI was detected in NGC 3226. In addition to the tidal tails, Mundell et al. (1995) discovered a $10^8 M_\odot$ cloud of HI close to, but physically and kinematically distinct from, the galactic disk of NGC 3227. They concluded this cloud was either a third galaxy in the interacting system being accreted by NGC 3227 or that it represented gas stripped from the disk of NGC 3227 and therefore was a candidate tidal

dwarf galaxy.

Here we present new ground-based broad-band BRI and narrow-band $H\alpha$ + $[NII]$ optical imaging, ultraviolet continuum imaging taken with the optical monitor on board XMM-Newton, and high angular resolution $\lambda 21$ -cm (HI) imaging of this candidate tidal dwarf galaxy, named hereafter J1023+1952. We also present 2-D $H\alpha$ ionized gas kinematics of this object and compare them with the HI kinematics. We assume a distance to the NGC 3227 system of 20.4 Mpc (Tully 1988); one arcsecond therefore corresponds to 99 pc.

2. OBSERVATIONS AND REDUCTION

2.1. $\lambda 21$ -cm HI Emission

The $\lambda 21$ -cm neutral hydrogen emission from the NGC 3227 system was imaged on 1995 November 26 and 30 using the Very Large Array (VLA) in B configuration. The total on-source observing time was 10.5 hours and data editing, calibration and analysis followed standard methods (e.g. Mundell et al. 1999). The final calibrated image cube has $1''.5$ pixels, a circular restoring beam size of $6''.3$ (624 pc), a velocity resolution of 10.3 km s^{-1} and an r.m.s. noise per channel of $0.3 \text{ mJy beam}^{-1}$. Moment analysis (e.g. Mundell et al. 1999) was performed on the image cube to isolate HI emission from the cloud J1023+1952, which is spatially and kinematically distinct from that of the disk of NGC 3227, and to derive images of the integrated HI intensity (Figure 1) and velocity structure of the cloud (Section 3.4).

2.2. Optical Continuum Imaging

NGC 3227 was imaged on 2000 February 5 with the Wide Field Camera (WFC) at the 2.5-m Isaac Newton telescope located on La Palma, Canary Islands. The WFC has a pixel scale of $0''.33$ per pixel. We obtained B, R and I images of $3 \times 1000 \text{ s}$, $2 \times 500 \text{ s}$ and $3 \times 300 \text{ s}$ exposure times respectively. The seeing was ~ 1 arcsec. Due to partial cloud cover through the night the final photometry was derived from values given for NGC 3227 in McAlary et al. (1983). The data reduction was carried out using standard IRAF tasks (e.g Miles et al. 2004, in prep). The B-band image of the interacting system is shown in Figure 3a; Figure 3b shows a close-up of the B-band image in the region of J1023+1952 with HI emission overlaid in contours.

2.3. H α Imaging and Spectroscopy

Narrow-band H α observations of NGC 3227 were obtained using the 4.2-m William Herschel Telescope on La Palma. The TAURUS filter centered at 6589 Å, width 15 Å, was used for a 600 s exposure; R-band continuum data were used for the continuum subtraction (Loiseau et al. in preparation). The pixel size is 0''.28. The quoted flux was the sum of the fluxes measured through four circular apertures centered on the H α -emitting regions co-spatial with J1023+1952 (Table 2) using the GAIA package.

H α spectroscopic images were obtained using the wide-field Fabry-Perot interferometer TAURUS-2¹ on the WHT (Loiseau et al. in preparation). After reduction and wavelength calibration the resulting data cube had dimensions of 500 x 500 x 60 pixels, a pixel size of 0''.54/pixel and channel separation of 14.1 km s⁻¹. The channel maps were combined to produce the H α velocity field (Section 3.4).

2.4. Ultraviolet Continuum Imaging

We obtained archival ultraviolet images taken on 2000 November 28 (P.I. Jansen) with the optical monitor on XMM-Newton in the UVM2 ($\lambda_c \sim 2298$ Å, $\Delta\lambda \sim 439$ Å) and UVW1 ($\lambda_c \sim 2905$ Å, $\Delta\lambda \sim 620$ Å) filters (see Mason et al. 2001). The exposure time for each filter was 1 ks, the pixel size is 0''.95 and the data were processed using SAS version 5.4. Measured counts in each filter were converted to flux units using a value averaged over different spectral types as listed in Section 7.1.2.8 (Method 2 by Breeveld) in the SAS Watchout documentation².

2.5. Infrared Continuum Imaging

Infrared images in J, H and K bands were obtained using the 1–5 μ m imager-spectrometer, UIST, on the UK Infrared Telescope (UKIRT) in imaging mode on 2003 May 25. Exposures were taken with the 180'' field of view (0''.12 pixels) centred on the location of J952+1026 and total integration times of 2220, 2220 and 3360 s in J, H and K bands respectively. Data reduction was performed using the ORAD-DR pipeline. Infrared emission was detected from the edge of the disk of NGC 3227 but no infrared emission was detected coincident with

¹(http://www.ing.iac.es/Astronomy/observing/manuals/html_manuals/wht_instr/taurus/taurus.html)

²(see http://xmm.vilspa.esa.es/external/xmm_sw_cal/sas.shtml)

J1952+1026.

3. DUST, GAS AND STARS IN J1023+1952

3.1. $\lambda 21$ -cm H I Emission

Figure 1(c) shows the high angular resolution image of the integrated H I emission from J1023+1952; the distribution of H I in the NGC 3227 system at lower resolution, taken from Mundell et al. (1995), is shown in Figures 1(a, b). J1023+1952 has an H I size of $\sim 90'' \times 60''$ ($8.9 \text{ kpc} \times 5.9 \text{ kpc}$) and significant structure is evident within the cloud with two prominent ridges of high N_{H} lying along P.A. $\sim 0^\circ$ in the northeast and P.A. $\sim 120^\circ$ in the south-west regions, hereafter: northern and southern ridges. More diffuse emission extends to the northeast and connects to the northern tidal tail reported by Mundell et al. (1995). Column densities in J1023+1952 are in the range of $\sim 4 \times 10^{20} < N_{\text{H}} < 4.0 \times 10^{21} \text{ cm}^{-2}$ (or $0.4 < A_B < 3.4 \text{ mag}$); the northern and southern ridges have similar N_{H} with the peak N_{H} occurring in the southern ridge (Figure 1(c)). H I emission is detected over the heliocentric velocity range 1188–1336 km s^{-1} with a full width at 20% intensity of the integrated H I profile of $W_{20} \sim 120 \text{ km s}^{-1}$. These H I properties are consistent with those measured by Mundell et al. (1995) from the lower resolution ($\sim 20''$) C-configuration dataset; the integrated H I emission measured from our new H I data is $\sim 12\%$ lower than that measured by Mundell et al. (1995) - a discrepancy that may be due to the inclusion of a small amount of faint extended emission from tidal tail gas in the value quoted by Mundell et al. (1995). Since the difference is small, we use the H I mass taken from Mundell et al. (1995) as an upper limit; correcting to a distance of 20.4 Mpc, the H I mass of J1023+1952 is therefore $M_{\text{H}} \sim 3.8 \times 10^8 M_\odot$.

3.2. Optical Continuum Emission

Figure 2 shows the combined BRI three-color image of the NGC 3227 system; continuum emission from NGC 3227 and NGC 3226 dominates the image and the two galaxies appear connected by a tidal arm curving anticlockwise from the southern point of the NGC 3227 disk to NGC 3226. A string of blue optically-emitting knots can be seen $\sim 70''$ ($\sim 7 \text{ kpc}$) west of the nucleus of NGC 3227; the string extends over $\sim 27''$ ($\sim 2.7 \text{ kpc}$) along P.A. $\sim 120^\circ$. Complex dust patches are also evident around and to the north east of the string of knots.

The blue knots and dust structures are prominent in the B-band image (Figure 3a); as can be seen in Figure 3b, the dust is co-spatial with the H I cloud J1023+1952 and, in

particular, the structure of the H I northern ridge closely matches that of the dust seen in the B-band image. In the southern half of J1023+1952, the string of blue knots coincides with the southern H I ridge.

The B–I color map in Figure 4 shows the dust structure and blue knots more clearly and, although no correction for intrinsic extinction has been applied, illustrates that the knots are bluer than any of the star formation regions in the disk of NGC 3227. Similarly the reddest region in J1023+1952, coincident with the northern H I ridge, is redder than the rest of the NGC 3227 disk at this radius; comparable reddening in NGC 3227 is only seen concentrated along the known bar close to the nucleus. The lack of stellar continuum in the NE of J1023+1952 and the close correspondence between H I-inferred values of A_B (~ 2.4 mag) and B–I color (~ 3 mag) in this region suggests that there is a significant quantity of dust intrinsic to J1023+1952 that is absorbing background stellar continuum emission from NGC 3227; we therefore suggest that the northern half of J1023+1952 is located in front of NGC 3227 along the line of sight. Numerical simulations of this interacting system could help to identify projection effects but are beyond the scope of this paper.

Table 1 lists the optical photometric parameters of the knots measured from the B, R and I images; the measurement apertures, listed in Columns (1) and (2), are shown in Figure 5. Columns (2)–(4) list the measured B, R, and I magnitudes in the given apertures; column (4) gives the (B–I) color corrected for Galactic extinction only and column (5) lists the corresponding M_B calculated using a distance modulus $|m - M| = 31.57$ (Tully 1988) and including correction for Galactic extinction. The tabulated values of M_B represent lower limits as the intrinsic extinction is not known but is likely to be high. As can be seen from Figure 3b, although the depth of the star-formation knots in the cloud along the line of sight is not known, the average intrinsic extinction could be as high as $A_B \sim 2$ mag, resulting in a total $M_B \sim -15.5$ mag, typical of tidal dwarf galaxies (e.g. Duc et al. 2000; de Oliveira et al. 2001). Column (7) shows the $(B-I)_0$ color corrected for Galactic extinction and additional intrinsic extinction corresponding to $A_B = 2$ mag.

3.3. Ultraviolet Continuum Emission

Figure 6 shows XMM-Newton ultraviolet images in the UVM2 and UVW1 filters of the NGC 3227 system. The blue knots in J1023+1952 are still prominent at ultraviolet wavelengths and, as can be seen in Figure 6a, are surrounded by a halo of diffuse UV emission that is coincident with the southern half of J1023+1952; comparable diffuse UV emission is markedly absent from the northern half of J1023+1952. The knots are also clearly detected at shorter wavelengths in the less-sensitive UVM2 image (Figure 6b). The total luminosity

L_{UV} ($\text{erg s}^{-1} \text{ \AA}^{-1}$) of J1023+1952 in each filter is listed in Table 2. The H I distribution and N_{H} in the northern and southern H I ridges in J1023+1952 are similar, leading to the conclusion that the absence of UV continuum emission from the northern half of J1023+1952 is due to an intrinsic lack of star formation in this region, rather than obscuration effects, and therefore vigorous star formation is isolated to the southern half of J1023+1952.

3.4. H α Emission and Kinematics

The presence of hot young stars in the south of J1023+1952 is further implied by the detection of H α emission from the blue continuum-emitting knots. Figure 7 shows the narrow-band H α image of the system in which H α emission from the active nucleus and from star-forming regions in the disk and bar of NGC 3227 is evident; H α emission coincident with the blue knots is indicated. The total measured H α flux is $2.55 \times 10^{-14} \text{ erg s}^{-1} \text{ cm}^{-2}$ corresponding to a star-formation rate (after Kennicutt 1998) of $\text{SFR} \sim 10.6 \times 10^{-3} \text{ M}_{\odot} \text{ yr}^{-1}$ that is uncorrected for intrinsic extinction.

The ionised gas kinematics, derived from the TAURUS Fabry Perot cube, are shown in Figure 8 along with the H I kinematics. The velocities of the H α knots lie in the range 1210–1348 km s^{-1} and are higher than those in the disk of NGC 3227 suggesting they are kinematically distinct. The corresponding H I velocities measured from the H I line profile at the location of the H α knots are $1290 \pm 46 \text{ km s}^{-1}$, closely matching those of the H α . This strongly suggests that the star-forming knots are embedded in J1023+1952 and are not merely optical knots in the background disk of NGC 3227.

3.5. Infrared Continuum Emission

No infrared emission was detected coincident with J1023+1952. Infrared emission was detected, as expected, from the edge of the disk of NGC 3227 providing a consistency check on the telescope pointing position. The lack of IR emission implies that the star formation knots are too young and blue to produce detectable IR emission and there is no prominent old stellar population. The $1\text{-}\sigma$ limiting surface brightness sensitivity for a 1-hour exposure at K-band is $22.8 \text{ mag arcsec}^{-2}$; integrating across the H I area of J1023+1952 and using relations in Campins, Rieke & Lebofsky (1985) and Thronson & Greenhouse (1988) for absolute K-band calibration and near infrared mass-to-light ratios in galaxies, we infer an upper limit to the old stellar population of $M_{\text{old}} < 9.4 \times 10^8 \text{ M}_{\odot}$ for J1023+1952.

4. DISCUSSION

The results presented in this paper and the H I kinematics presented by Mundell et al. (1995) demonstrate that J1023+1952 is physically and kinematically distinct from the disk of NGC 3227 and lies in the foreground between us and the background disk of NGC 3227. The close correspondence between the H α and H I velocities provides strong evidence that the star-forming knots are embedded in J1023+1952 and are not merely optical knots in the background disk of NGC 3227, confirming the suggestion of Mundell et al. (1995) that this H I cloud is a dwarf galaxy. Here we discuss the possible origin of this dwarf galaxy as either a third, pre-existing dwarf galaxy involved in the interaction with NGC 3227 and NGC 3226, or a newly-forming dwarf galaxy condensing out of the tidal debris removed from the gaseous disk of NGC 3227. Whatever the origin of J1023+1952, we suggest that we are witnessing shock-triggered star formation in infalling tidal material and that this may provide a mechanism for the formation of young extragalactic/intracluster H II regions.

4.1. J1023+1952 – Pre-existing Dwarf or Young Tidal Dwarf Galaxy?

One scenario for the origin of J1023+1952 is that it is a pre-existing dwarf galaxy involved in the interaction with NGC 3227 instead of, or in addition to NGC 3226; as suggested by Mundell et al. (1995), in this scenario the tidal forces in a prograde encounter would have caused the northern tail to be extracted from J1023+1952 and the southern tail to be extracted from NGC 3227, in a manner similar to other known encounters in which two gas-rich galaxies interact and each galaxy develops one tidal tail (e.g. Toomre & Toomre 1972). NGC 3227 is the brightest member of a galaxy group variously classified to contain between four and thirteen members (Huchra & Geller 1982; Garcia 1993; Ramella, Pisani & Geller 1997); in this wider group environment in which galaxy evolution is ongoing, it is not unreasonable to expect to find pre-existing dwarf galaxies (Zabludoff & Mulchaey 2000).

Alternatively, J1023+1952 may be newly formed from tidal debris stripped from the disk of NGC 3227; the presence of blue optical knots along tidal tails in interacting galaxy systems has long been recognised as an indication that condensations of tidal debris, ejected during an interaction, might evolve into dwarf galaxies (e.g. Zwicky 1956; Schweizer 1978; Mirabel, Dottori & Lutz 1992). Indeed, a chain of star-formation knots, with similar optical properties to J1023+1952, is observed in the TDG at the end of the southern tidal tail in NGC4038/39 (Mirabel et al. 1992).

The blue colors, large H α equivalent widths and the presence of ultraviolet emission in J1023+1952 suggests star formation is dominated by hot young stars, in particular late-

O/early-B stars with lifetimes $< 10^8$ yr. Comparison of our measured UV luminosities with those predicted by Starburst99 models (Leitherer et al. 1999) for an instantaneous burst of star formation (including nebular continuum), suggests a star-burst age < 10 Myr for the knots in J1023+1952; the high $H\alpha$ equivalent width of $\sim 283\text{\AA}$ is also consistent with a strong burst of star formation less than 10 Myr ago (Alonso-Herrero et al. 1996). Mendes de Oliveira et al. (2001) used $H\alpha$ and blue luminosities to derive star formation rates for tidal dwarf galaxy candidates in Stephan’s Quintet. The $H\alpha$ and blue luminosities of J1023+1952, uncorrected for intrinsic extinction (see Table 2), imply a star-formation rate of $\text{SFR}(H\alpha) \gtrsim 10.6 \times 10^{-3}$ and $\text{SFR}(L_B) \gtrsim 1.1 \times 10^{-3} M_\odot \text{ yr}^{-1}$ similar to giant HII regions (Mayya 1994; Figure 6 in Mendes de Oliveira et al 2001); correcting for extinction results in star formation rates similar to those of both blue compact galaxies (BCDs) (Sage et al. 1992) and tidal dwarf candidates in Stephan’s Quintet (Mendes de Oliveira et al 2001). Although the HI mass and HI linewidth measured for J1023+1952 (see Table 2) are similar to those measured for some BCDs (van Zee, Skillman & Salzer 1998), the 8.9-kpc HI diameter of J1023+1952 is larger than those typical of BCD ($\lesssim 2$ kpc); the distribution of HI and star formation is also less centrally concentrated in J1023+1952 than in BCDs. Tidal effects might explain these discrepancies, but a striking property of J1023+1952 is its apparent lack of an old stellar population (Section 3.5), making it an unusual dwarf galaxy if pre-existing (Cairós et al. 2003). In the context of tidal dwarf galaxies, the observed HI mass, column density, extent and global kinematics of J1023+1952 (Tables 1 and 2) are broadly consistent with the range of properties known for other confirmed tidal dwarf galaxies (Mirabel et al. 1992; Duc & Mirabel 1994; Hibbard et al. 1994; Duc et al. 2000; Braine et al. 2001; Mendes de Oliveira et al. 2001) and the lack of an old stellar population could be understood if J1023+1952 is newly formed from gaseous tidal debris removed from NGC 3227.

A key difference between classical dwarfs and TDGs is metallicity. Unlike classical dwarf galaxies which follow a luminosity-metallicity relation, the metallicities of TDGs appear to lie in a narrow range $12+\log(\text{O}/\text{H}) = 8.3\text{--}8.7$ (Duc et al. 2000; Lisenfeld et al. 2002; Duc, Bournaud & Masset 2004) reflecting their origin as enriched material tidally stripped from a progenitor galaxy disk. For the absolute magnitude of $M_B = -13.5$, the galaxy metallicity-luminosity (Z-L) relation (e.g. Brodie & Huchra 1991) would predict a metallicity of $[\text{Fe}/\text{H}] \sim -2$ for J1023+1952. If, however, the gas in J1023+1952 came from the disk of NGC 3227, it would be enriched to approximately solar metallicity and hence deviate from the classic Z-L relation, following other TDGs (Weilbacher et al. 2003). The location of J1023+1952 on the Z-L relation will therefore discriminate between J1023+1952 as a pre-existing or newly-formed dwarf galaxy.

4.2. Dark matter in J1023+1952?

Simulations of interacting disk galaxies with dark halos (Barnes & Hernquist 1992) produced tidal concentrations with less than 5% of their mass in dark matter, predicting that tidal dwarf galaxies, in contrast to classical dwarf galaxies, should have low mass-to-light ratios. Braine et al. (2001) confirmed this prediction with detection of a significant quantity of CO in eight gas-rich TDGs. The HI distribution and kinematics of J1023+1952 are suggestive of a rotating disk structure, but the contribution of projection effects on the observed structure cannot be ruled out. Assuming the neutral gas is distributed in a circularly-rotating disk of radius ~ 4.45 kpc the observed velocity gradient implies a dynamical mass of $M_D \sim 3.6 \times 10^9 (\sin^{-2} i) M_\odot$, suggesting that HI accounts for $\sim 11\%$ of the total mass. Correcting the measured HI mass for the presence of He such that $M_{\text{gas}} = 1.34 * M_H$ (after Hunter et al. 2000) and deriving the mass in stars $M_{\text{star}} = 1.54 * L_B$ (assuming intrinsic extinction $A_B=2$), we conclude that the mass in gas and stars ($M_{\text{gas}} + M_{\text{star}}$) accounts for at least 24% of the dynamical mass of J1023+1952; inclusion of the old stellar population mass upper limit of $9.4 \times 10^8 M_\odot$ takes this value to $\sim 50\%$. Therefore, if J1023+1952 is gravitationally bound, the measured dynamical mass would require a detection of a significant quantity of molecular gas to exclude the presence of dark matter, given the lack of any obvious old stellar component. Alternatively, as suggested by the young star-formation age, J1023+1952 might not yet be fully self-gravitating and the large HI linewidth could then be explained by a velocity gradient of infalling tidal gas rather than rotation. Measurement of the molecular gas mass, distribution and kinematics will provide useful constraints on the dynamics of J1023+1952 and its current evolutionary state.

4.3. A Dynamical Trigger for the Star Formation in J1023+1952

There appears to be an empirical relationship between observed HI column densities and the presence of star formation in galaxies (e.g. Duc et al. 2000). The star-formation threshold is $N_H \sim 0.5 - 1 \times 10^{21} \text{ cm}^{-2}$ in dwarf galaxies and low surface brightness galaxies (e.g. Gallagher & Hunter 1984; Skillman 1987; van der Hulst et al. 1993; van Zee et al. 1997) but Martin & Kennicutt (2001) find that a high gas surface density alone is not sufficient to predict the presence of star formation in a galaxy disk and suggest that an additional dynamical trigger is required for the onset of star formation. Elmegreen et al. (1993) argued that large velocity dispersions in the ISM, induced by tidal agitation, can result in the formation of massive gas clouds similar to J1023+1952, with high internal dispersion and high star formation efficiency. The velocity dispersion of HI in J1023+1952 of $\sigma \sim 25-30 \text{ km s}^{-1}$ is consistent with that found by Elmegreen et al. (1993) to result in

the formation of large clouds with masses in excess of $10^8 M_\odot$. Barnes (2004) also argues that density-dependent star formation rules are insufficient and suggests a dynamical trigger in which star formation is governed by the local rate of energy dissipation in shocks.

A dynamical trigger would appear to be necessary to explain why the star formation in J1023+1952 is localised to the southern half of the H I cloud, given the similarity in N_{H} in the southern and northern H I ridges. If J1023+1952 is forming from infalling tidal debris, then the southern ridge in J1023+1952 could represent a shock in the returning material where gas is compressed to sufficiently high gas densities to trigger the observed star formation. Such a shock would compress the gas in the southern ridge resulting in a region in which both molecular and atomic densities are high, with the molecular gas forming *in situ* and providing both the fuel for the star formation and the necessary shielding from the resultant UV radiation (Allen et al. 1997). A similar region of active star formation has also been observed at the base of the tidal tail of NGC 4676b (e.g. de Grijs et al. 2003) - a member of the interacting galaxy pair NGC 4676 (“The Mice”). Simulations of star formation in this system (Barnes 2004) show that star formation occurs in a shock produced as gas from the curved tail falls back into its original disk. The presence of broad H I linewidths across J1023+1952 and, in particular, broad, double-peaked H I and H α lines along the southern H I ridge further supports a turbulent, shock scenario for the triggering of the observed star formation; detection of molecular gas localized to the southern ridge in J1023+1952 with similar kinematic properties to those of the H I and H α components would provide additional support for the shock hypothesis.

In the context of TDG formation, the location of J1023+1952 at the base of the northern tidal tail is unusual. Duc et al. (2000) argue that, if a TDG is defined as a long-lived, gravitationally-bound object, the most probable location for them to be observed is towards the tips of a tidal tails since TDGs formed close to the progenitor would disappear quickly (Mirabel et al. 1992; Duc et al. 2000; Bournaud, Duc & Masset 2003). Indeed, dynamical simulations of the merging system NGC 7252 (Hibbard & Mihos 1995) show that material at the base of a tidal tail is more tightly bound to the progenitor than material at the ends and falls back quickly to small pericentric distances, with debris at greater distances falling back more slowly to correspondingly greater pericentric distances. The rate of return of tidal debris scales as $t^{-5/3}$, implying a high initial rate of return with as much as 50% of the tidally-stripped material falling back to the progenitor nucleus after only 175 Myr (Hibbard & Mihos 1995). As the projected distance between NGC 3227 and J1023+1952 along the line of sight is not known, we cannot constrain whether J1023+1952 is stable to tidal disruption and therefore likely to be long-lived. Nevertheless Mundell et al. (1995) note that the H I distribution of the disk of NGC 3227 is asymmetrical with less H I on the side close to J1023+1952, suggesting the northern tail (and hence the material in J1023+1952) originated

from NGC 3227. Therefore, if the northern H I tidal tail represents material stripped from the disk of NGC 3227 and J1023+1952 is forming from returning tidal debris, the dynamical age of J1023+1952 would be younger than 100 Myr - consistent with the derived star formation age.

Whether J1023+1952 is a pre-existing dwarf galaxy, a young TDG or a transient galaxy-like object, the discovery of vigorous ongoing star formation outside of the disks of interacting galaxies such as NGC 3227, suggests that the gas dynamics in such environments are suitable for the shock-triggering of extragalactic star formation and may provide a mechanism for the formation of young intergalactic HII regions similar to those discovered by Gerhard et al. (2002) and Ryan-Weber et al. (2004).

5. Conclusions

We have used multi-wavelength imaging and spectroscopy to investigate the nature of the massive H I cloud, originally identified by Mundell et al. (1995) in the interacting Seyfert system NGC 3227/3226 and named J1023+1952 in this paper. We find:

- Two H I ridges in the northern and southern halves of the cloud, with comparable H I column densities in the range $\sim 4 \times 10^{20} < N_{\text{H}} < 4.0 \times 10^{21} \text{ cm}^{-2}$ (or $0.4 < A_B < 3.4 \text{ mag}$).
- A string of blue, H α -emitting knots of star formation, coincident with the southern H I ridge, with an extent of $\sim 2.7 \text{ kpc}$, total magnitude $M_B \sim -15.5 \text{ mag}$ (assuming a conservative estimate for the internal extinction of $A_B \sim 2$ derived from the observed N_{H}) and an H α luminosity $L_{\text{H}\alpha} > 1.35 \times 10^{39} \text{ erg s}^{-1}$.
- Ultraviolet continuum emission from the knots, a halo of diffuse UV continuum emission around the southern half of J1023+1952 and UV luminosities and H α equivalent widths consistent with a burst of instantaneous star formation less than 10 Myr ago.
- Closely matched ionised and neutral gas kinematics in the southern half of J1023+1952 with $1210 < V_{\text{H}\alpha} < 1348 \text{ km s}^{-1}$ and $V_{\text{HI}} \sim 1290 \pm 46 \text{ km s}^{-1}$, confirming unambiguously that the newly-discovered star formation is occurring *in situ* in the southern half of the cloud, rather than in the underlying disk of NGC 3227.
- A lack of UV and optical emission from the northern half of J1023+1952 and a close match between the inferred reddening and spatial distribution of dust and H I in the northern ridge, confirming that the northern half of the cloud lacks star formation and

is seen primarily in absorption against the background stellar continuum from the disk of NGC 3227.

We conclude that J1023+1952 exhibits properties broadly consistent with dwarf galaxies, whether pre-existing or tidal in origin; the lack of a detectable old stellar population in J1023+1952 makes a tidal origin more likely but measurements of metallicity are required to confirm this. We speculate that if J1952+1052 is tidal in origin, its unusual location at the base of the northern tidal tail and the localization of star-formation to its southern HI ridge suggest that it is young and forming from gaseous material tidally stripped from the disk of NGC 3227 that is in the first stages of infall. We suggest the southern ridge might represent a shock that has formed in gas as it falls back along the northern tail onto the progenitor disk, triggering the observed star formation. Such early TDGs are thought to be rare due to the rapid fall-back timescale of material close to the progenitor, suggesting a dynamical age $\tau < 100$ Myr for J1023+1952, consistent with its derived star-formation age.

CGM acknowledges financial support from the Royal Society. We are grateful to J. Barnes for allowing us to cite his paper before publication and thank the referee for helpful suggestions that improved the paper. The National Radio Astronomy Observatory is a facility of the National Science Foundation operated under cooperative agreement by Associated Universities, Inc. This research has made use of NASA’s Astrophysics Data System Abstract Service (ADS) and the NASA/IPAC Extragalactic Database (NED), which is operated by the Jet Propulsion Laboratory, California Institute of Technology, under contract with the National Aeronautics and Space Administration. The WHT and INT are operated on the island of La Palma by the Isaac Newton Group in the Spanish Observatorio del Roque de los Muchachos of the Instituto de Astrofísica de Canarias. The United Kingdom Infrared Telescope is operated by the Joint Astronomy Centre on behalf of the UK Particle Physics and Astronomy Research Council.

REFERENCES

- Allen, R.J., Knapen, J.H., Bohlin, R. & Stecher, T.P. 1997, *ApJ*, 487, 171
- Alonso-Herrero, A., Aragon-Salamanca, A., Zamorano, J. & Rego, M. 1996 *MNRAS*, 278, 417
- Barnes, J. & Hernquist, L. 1992 *ARA&A*, 30, 705
- Barnes, J.E 2004 *MNRAS*, 350, 798

- Bournaud, F, Duc, P.-A. & Masset, F. 2003 A&A, 411, L469
- Braine, J., Duc, P.-A., Lisenfeld, U., Charmandaris, V., Vallejo, O., Leon, S. & Brinks, E. 2001 A&A, 378, 51
- Brodie J. & Huchra J. 1991, ApJ, 379, 157
- Burkey, J.M., Keel, W.C., Windhorst, R.A. & Franklin, B.E. 1994, ApJ, 429, L13
- Campins, H., Rieke, G.H. & Lebofsky, M.J. 1985 AJ, 90, 896
- Cairós, L.M.; Caon, N., Papaderos, P., Noeske, K., Vílchez, J.M., Lorenzo, B.G. & Muñoz-Tuñón, C. 2003 ApJ, 593, 312
- Cowie, L.L., Songaila, A., Hu, E.M. & Cohen, J.G. 1996, AJ, 112, 839
- de Grijs, R., Lee, J.T., Clemencia Mora Herrera, M., Fritze- v. Alvensleben, U. & Anders, P. 2003, New Astr. 8, 155
- Duc, P.-A. & Mirabel, I.F. 1994, A&A, 289, 83
- Duc, P.-A., Brinks, E., Springel, V., Pichardo, B., Weilbacher, P. & Mirabel, I.F. 2000, AJ, 120, 1238
- Duc, P.-A., Bournaud, F. & Masset, F. 2004, in IAU Symposium 217, "Recycling intergalactic and interstellar matter", eds. Duc, P. A., Braine, J., Brinks, E., ASP, in press (astro-ph/0402252)
- Elmegreen, D.M., Kaufman, M. & Thomasson, M. 1993, ApJ, 412, 90
- Gallagher, J.S. & Hunter, D.A. 1984, ARA&A, 22 37
- Garcia, A.M. 1993 A&AS, 100, 47
- Gerhard, O., Anaboldi, M., Freeman, K.C. & Okamura, S. 2002, ApJ, 580, L121
- Hibbard, J.E., Guhathakurta, P., van Gorkom, J.H. & Schweizer, F. 1994 AJ, 107, 67
- Hibbard, J.E. & Mihos, J.C. 1995 AJ, 110, 140
- Huchra, J.P. & Geller, M.J. 1982 ApJ, 257, 423
- Hunsberger, S.D., Charlton, J.C. & Zaritsky, D. 1996, ApJ, 462, 50
- Hunter, D.A., Hunsberger, S.D. & Roye, E.W. 2000, ApJ, 542, 137

- James, P.A., Shane, N.S., Beckman, J.E. et al. 2004, *A&A*, 414, 23
- Kennicutt, R.C. 1998, *ARA&A*, 36, 189
- Leitherer, C., Schaerer, D., Goldader, J.D., González-Delgado, R.M., Robert, C., Kune, D.F., de Mello, D.F., Devost, D. & Heckman, T.M. 1999, *ApJS*, 123, 3
- Lisenfeld, U., Braine, J., Vallejo, O., Duc, P.-A., Leon, S., Brinks, E. & Charmandaris, V. 2002, in "Modes of Star Formation and the Origin of Field Populations", eds. E.K. Grebel & W. Brandner, *ASP Conf. Series Vol. 285*, 406
- Martin, C.L. & Kennicutt, R.C. 2001, *ApJ*, 555, 301
- Mason, K.O., Breeveld, A., Much, R. et al. 2001, *A&A*, 365, L36
- Mayya, Y.D. 1994, *AJ*, 108, 1276
- McAlary, C.W., McLaren, R.A., McGonegal, R.J. & Maza, J. 1983, *ApJS*, 52, 341
- Mendes de Oliveira, C., Plana, H., Amram, P., Balkowski, C. & Bolte, M. 2001, *AJ*, 121, 2524
- Mirabel, I.F., Dottori, H. & Lutz, D. 1992 *A&A*, 256, L19
- Mihos, C. 2001 *ApJ*, 550, 94
- Mundell, C.G., Pedlar, A., Axon, D.J., Meaburn, J. & Unger, S.W. 1995, *MNRAS*, 277, 641
- Mundell, C.G., Pedlar, A., Shone, D.L. & Robinson, A. 1999 *MNRAS*, 304, 481
- Ramella, M., Pisani, A. & Geller, M.J. 1997 *AJ*, 113, 483
- Ryan-Weber, E.V. et al. 2004 *AJ*, 127, 1431
- Sage, L.J., Saltzer, J.J., Loose, H.-H. & Henkel, C. 1992, *A&A*, 265, 19
- Schweizer, F. 1978, in "Structure and Properties of Nearby Galaxies", *IAU Symp. 77*, 279
- Skillman, E.D. 1987, in "Star Formation in Galaxies", ed. C.J. Lonsdale Persson, *NASA, CP-2466*, p. 263
- Staveley-Smith, L. & Davies, R.D. 1987, *MNRAS*, 224, 953
- Struck, C. 1999, *Ph. R.*, 321, 1
- Thronson H.A., Jr. & Greenhouse, M.A. 1988 *ApJ*, 325, 604

- Toomre, A. & Toomre, J. 1972, ApJ 178, 623
- Tully, R.B. 1988, Nearby Galaxies Catalog (Cambridge: Cambridge Univ. Press)
- van der Hulst, J.M., Skillman, E.D., Smith, T.R., Bothun, G.D., McGaugh, S.S. & de Blok, W.J.G. 1993, AJ, 106, 548
- van Zee, L., Haynes, M.P., Salzer, J.J. & Broeils, A.H. 1997, AJ, 113, 1618
- van Zee, L., Skillman, E.D. & Salzer, J.J. 1998 AJ, 116, 1186
- Weilbacher, P.M., Duc, P.-A., Fritze-v. Alvensleben, U. 2003, A&A, 397, 545
- Zabludoff, A.I. & Mulchaey, J.S. 2000, ApJ, 539, 136
- Zwicky, F. 1956, Erge. Exacten Naturwiss., 29, 344

Table 1: BRI aperture photometry (see Figure 5 for apertures)

ID	Aperture Diameter (arcsec)	B (mag)	R (mag)	I (mag)	$(B - I)$ (mag)	M_B (mag)	$(B - I)_0$ (mag)
(1)	(2)	(3)	(4)	(5)	(6)	(7)	
#1	3.46	20.67	19.75	19.49	1.13	−11.0	0.03
#2	4.58	19.89	19.16	18.63	1.21	−11.8	0.11
#3	4.49	21.30	20.13	19.53	1.72	−10.4	0.62
#4	2.97	21.69	20.47	19.86	1.78	−10.0	0.68
#5	6.14	20.74	19.54	18.80	1.89	−10.9	0.79
#6	29.1 ^a	18.16	16.98	16.48	1.63	−13.5	0.53

^aEllipse eccentricity is 0.83

Table 2: Derived Properties for J1023+1952

α (J2000)	10h 23m 26 ^s .5
δ (J2000)	19° 52′ 0″.0
H I Diameter (kpc)	8.9
M_H (M_\odot)	3.8×10^8
Systemic Velocity (km s^{-1})	~ 1270
W_{20} (km s^{-1})	120
Dynamical Mass M_D (M_\odot)	3.6×10^9
Star-formation Extent (kpc)	2.7
^a Total M_B (mag)	−13.5
H α Equivalent Width (\AA)	283
^a Total $F_{H\alpha}$ ($\text{erg s}^{-1} \text{ cm}^{-2}$)	2.55×10^{-14}
^a Total $L_{H\alpha}$ (erg s^{-1})	1.35×10^{39}
^a Total L_B (L_\odot)	3.9×10^7
^a Total $L_{\lambda_{2905} \text{ \AA}}$ ($\text{erg s}^{-1} \text{ \AA}^{-1}$)	5.6×10^{38}
^a Total $L_{\lambda_{2298} \text{ \AA}}$ ($\text{erg s}^{-1} \text{ \AA}^{-1}$)	7.5×10^{36}

^aUncorrected for extinction

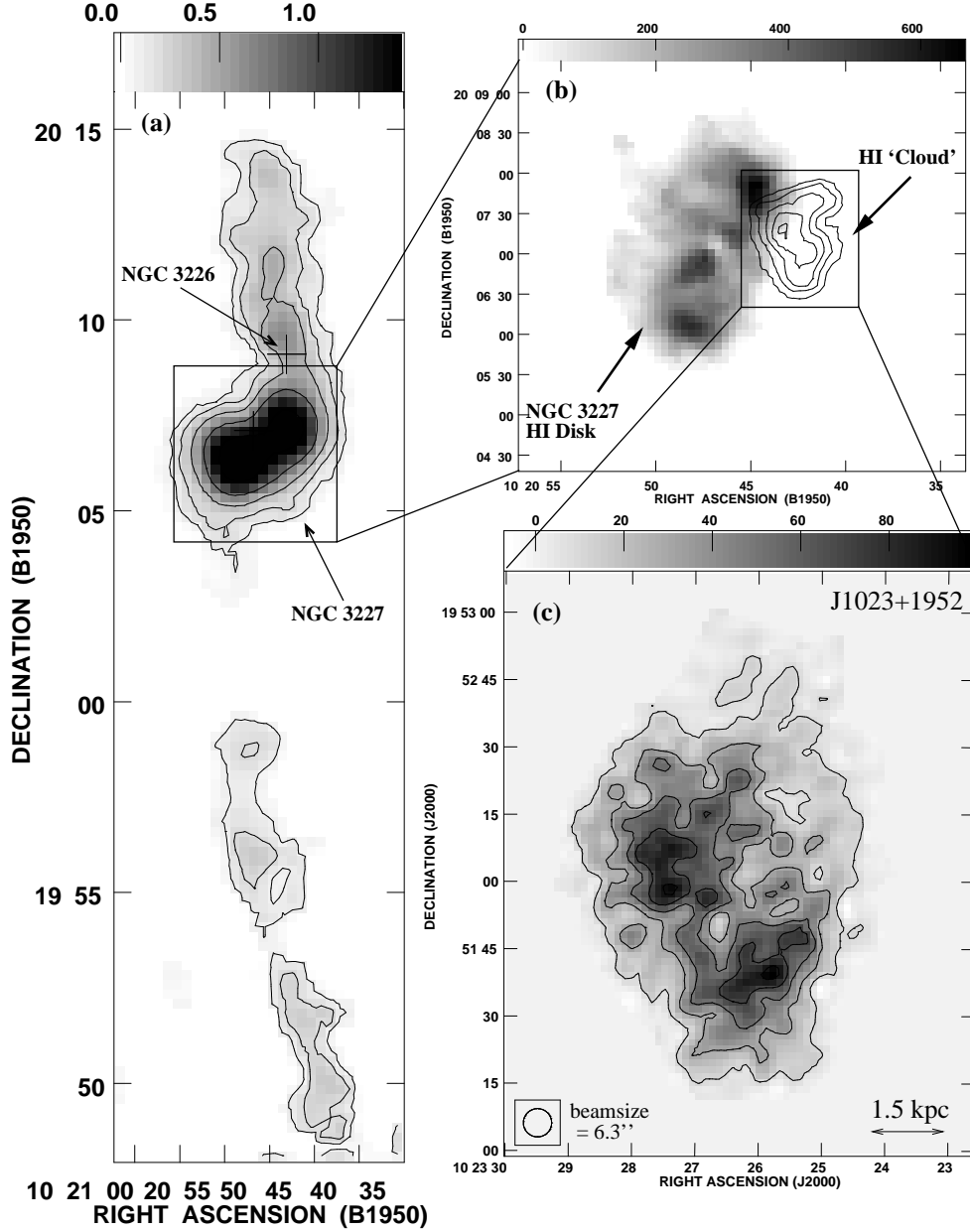


Fig. 1.— (a) VLA D-configuration HI image (zeroth moment) of the NGC 3227 system (from Mundell et al. 1995); the angular resolution is $60''.7 \times 58''.2$ and the location of NGC 3226 is indicated by ‘+’; (b) VLA C-configuration HI imaging that resolved HI emission from the disk of NGC 3227 and the ‘HI cloud’ (Mundell et al. 1995); the angular resolution is $20''.5 \times 18''.3$; (c) new B-configuration image of integrated hydrogen emission from the dwarf candidate, J1023+1952. The angular resolution is $6''.3 \times 6''.3$ and contour levels correspond to column densities $N_{\text{H}} = (0.4, 1.2, 2.1, 2.9, 3.7) \times 10^{21} \text{ cm}^{-2}$; peak $N_{\text{H}} = 4.0 \times 10^{21} \text{ cm}^{-2}$.

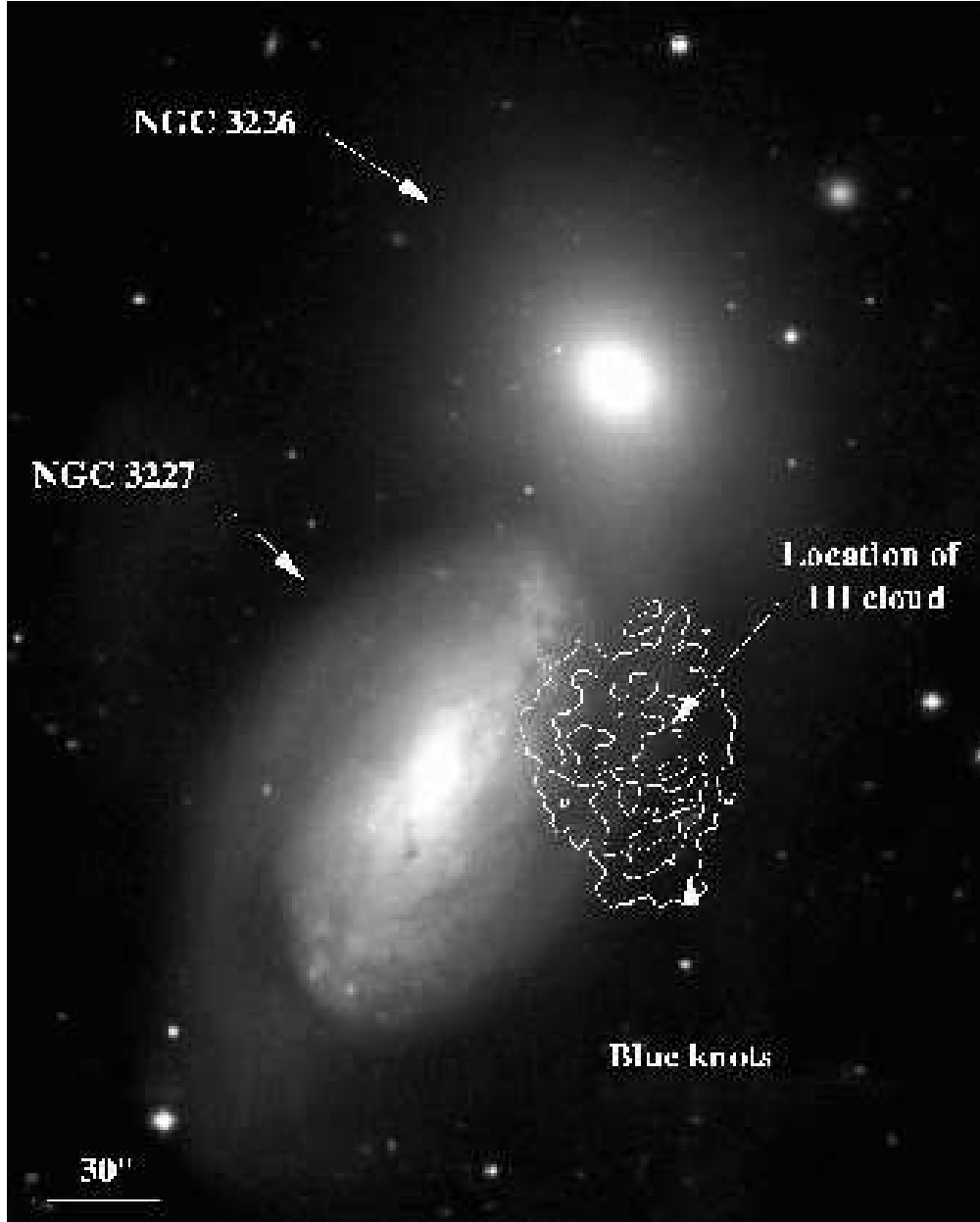


Fig. 2.— Three-color image of the NGC 3227/3226 system. B,R, and I images are in blue, green and red channels respectively. Contours of H I emission from J1023+1952 are overlaid in white.

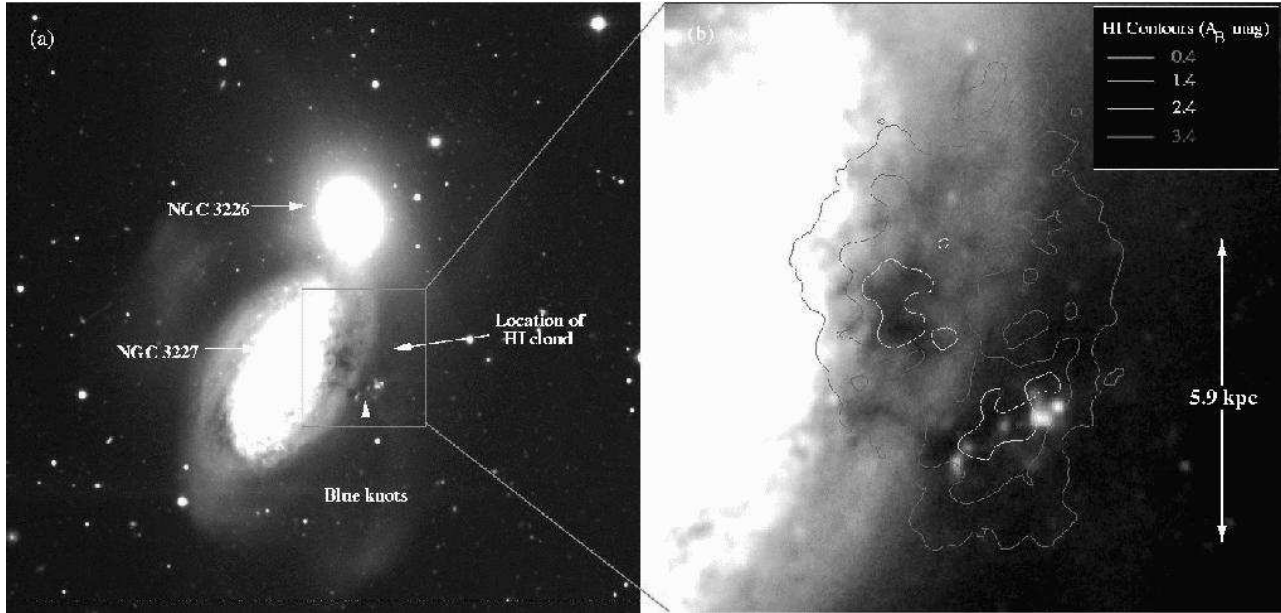


Fig. 3.— (a) INT *B*-band image; the location of H I cloud J1023+1952 and string of newly-discovered blue knots are indicated. (b) contours of H I emission from J1023+1952 overlaid on *B*-band image showing a close correspondence between the high column-density H I ridges and the string of blue knots and dust patch. Contours correspond to N_{H} converted to magnitudes of optical *B*-band extinction assuming a Galactic extinction law (Stavely-Smith & Davies 1987).

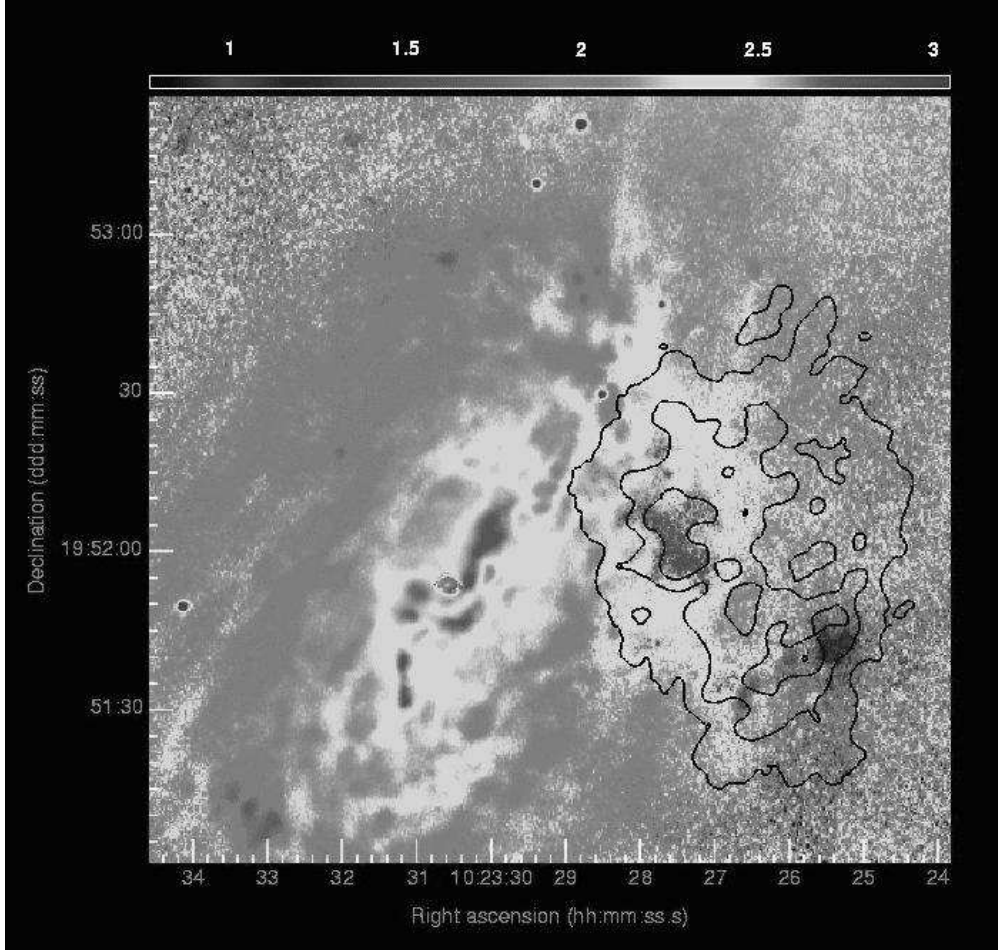


Fig. 4.— INT B–I image, corrected for Galactic extinction, with H I contours overlaid. The color scale in magnitudes is indicated at the top of the image; no correction for intrinsic extinction has been applied. The H I contour levels correspond to $A_B = 0.4, 1.4, 2.4, 3.4$ mag (as in Figure 3b) .

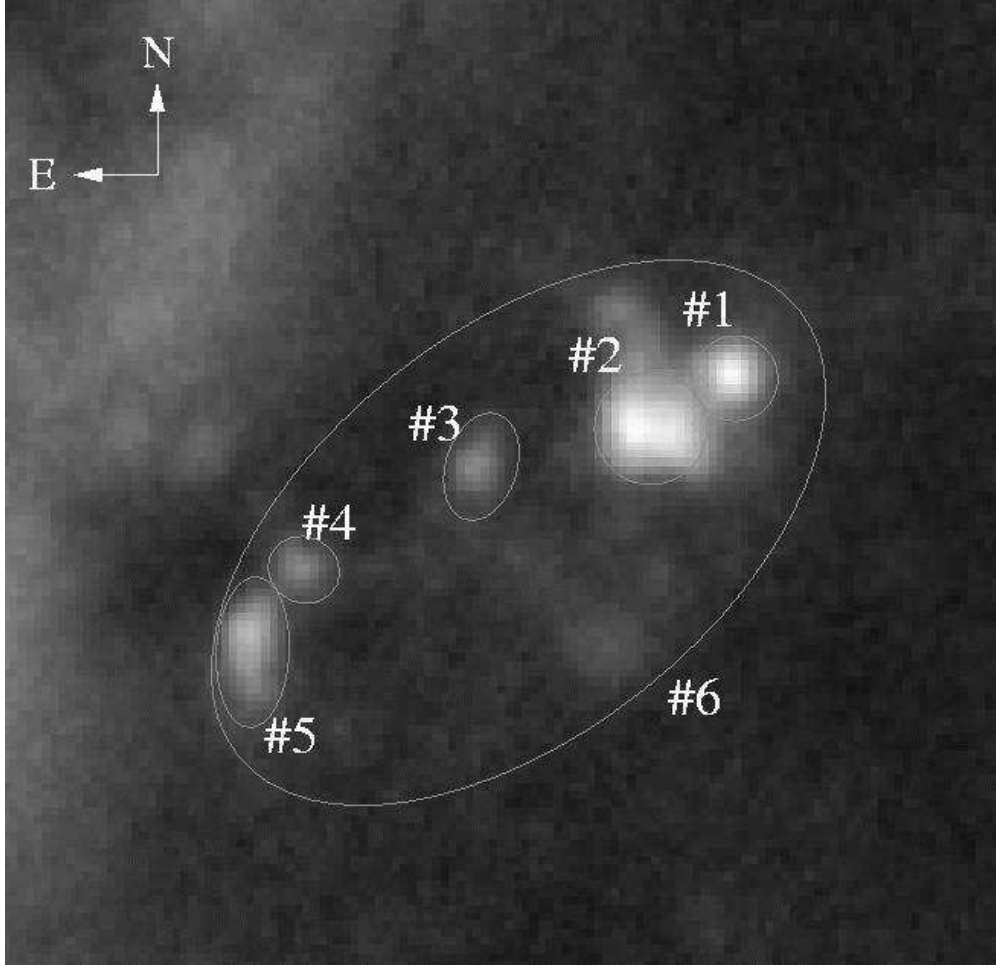


Fig. 5.— INT *B*-band image: apertures used to measured photometry of knots in BRI images as listed in Table 1. Aperture 6 has a major axis extent of $29''$.

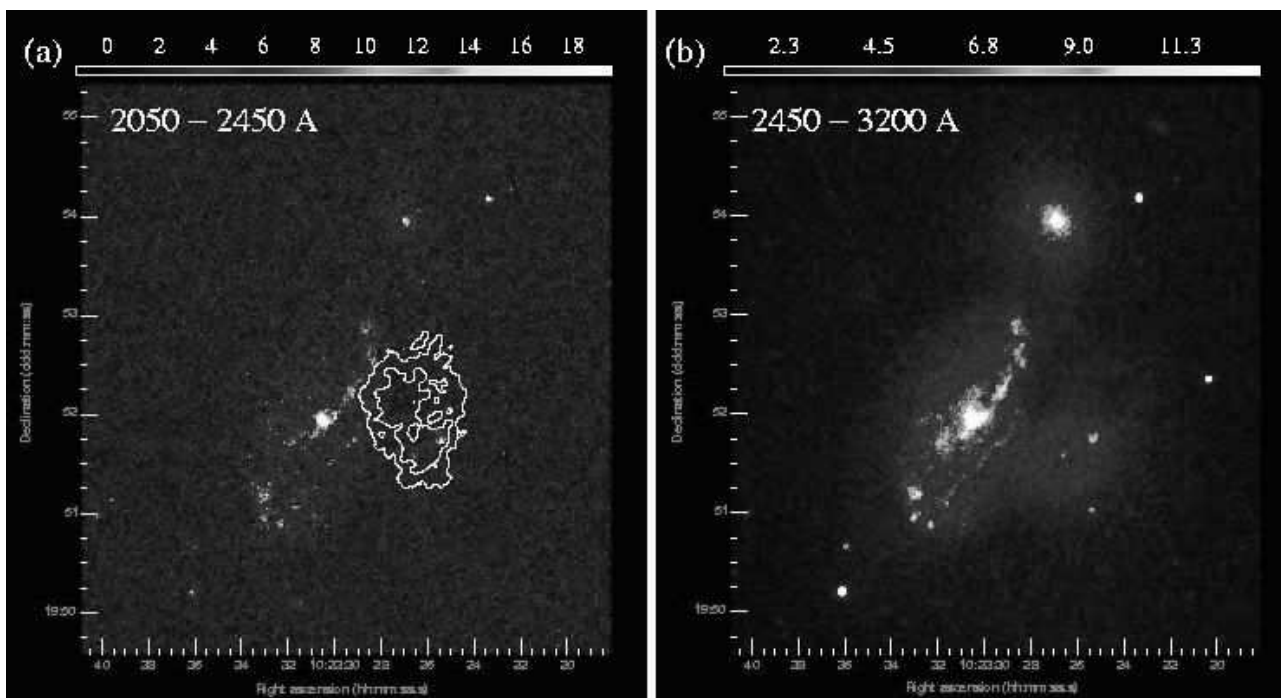


Fig. 6.— XMM-Newton ultraviolet images of the NGC 3227 system in the (a) UVM2 filter with H I contours overlaid (b) UVW1 filter. Flux density scales are given in units of (a) $10^{-16} \text{ erg s}^{-1} \text{ Å}^{-1} \text{ cm}^{-2}$ and (b) $10^{-15} \text{ erg s}^{-1} \text{ Å}^{-1} \text{ cm}^{-2}$.

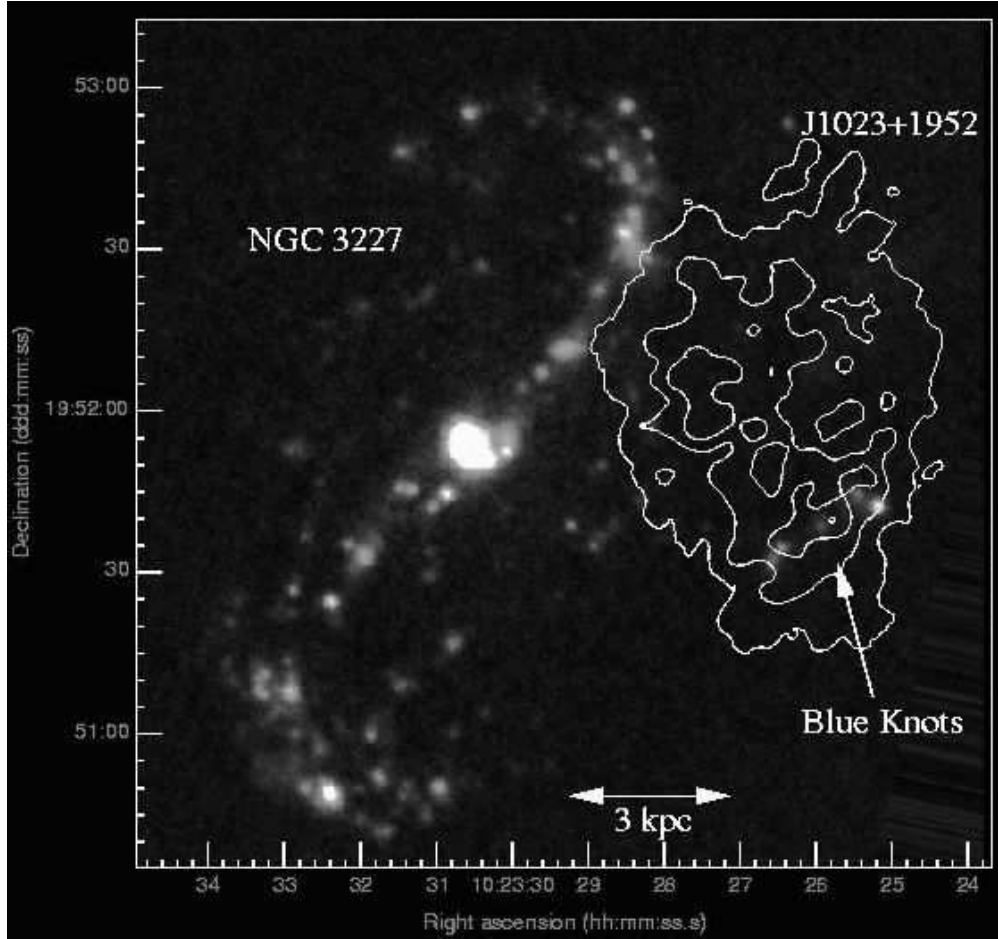


Fig. 7.— WHT narrow-band H α image of the NGC 3227 system; H I contours of J1023+1952 are overlaid.

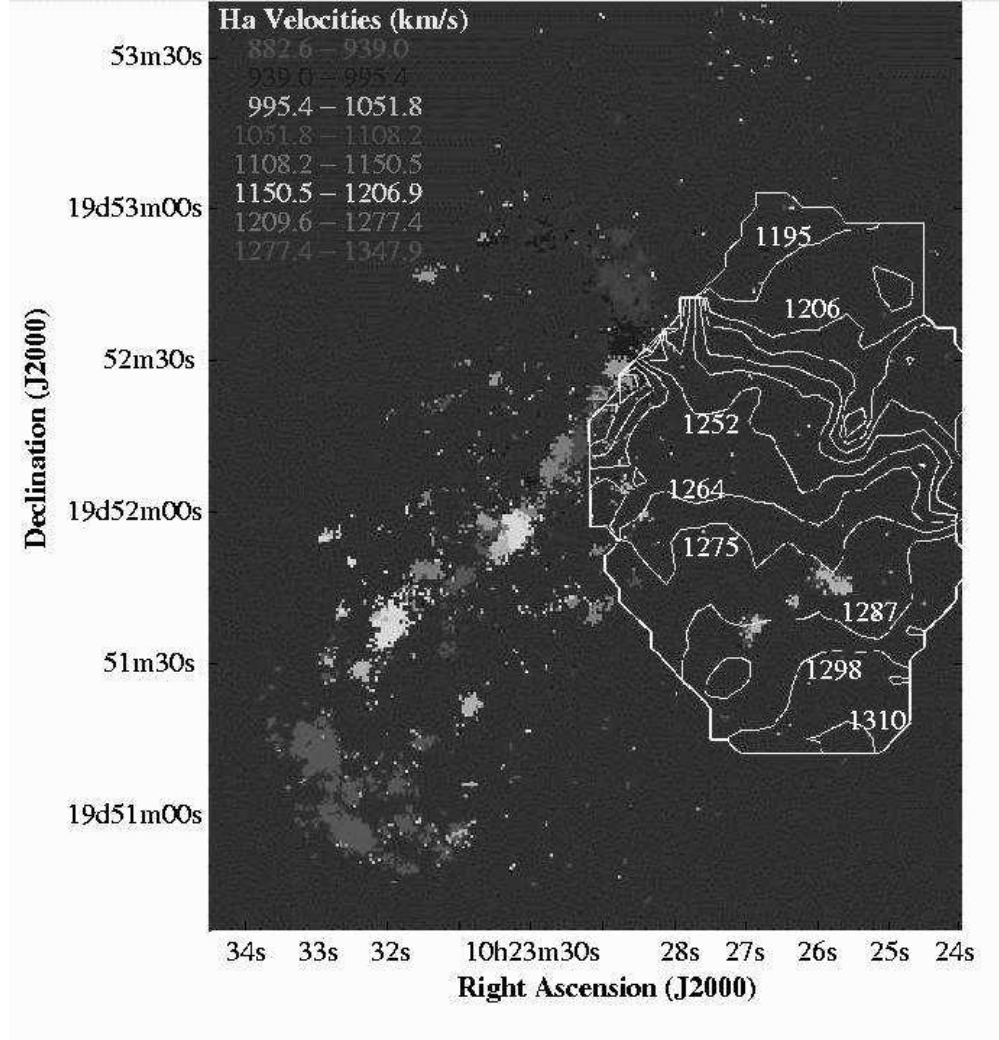


Fig. 8.— TAURUS H α velocity field (color) of the NGC 3227 system; HI isovelocity contours for J1023+1952 are superimposed in white and labelled in units of km s⁻¹.